Chin. Geogra. Sci. 2012 Vol. 22 No. 1 pp. 48–62
doi: 10.1007/s11769-012-0513-5
www.springerlink.com/content/1002-0063

Grain-size Characteristics and Climate Variability in TMS5e Sequence of Tumen Section in Southern Tengger Desert, Northwestern China

WEN Xiaohao[1], LI Baosheng[1, 2], WANG Fengnian[1], ZHENG Yanming[3], NIU Dongfeng[1], SI Yuejin[1], OU Xianjiao[1, 4]

(*1. School of Geographical Science, South China Normal University, Guangzhou 510631, China; 2. State Key Laboratory of Loess and Quaternary Geology, Institute of Earth Environment, Chinese Academy of Sciences, Xi'an 710075, China; 3. School of Geography and Planning, Sun Yat-Sen University, Guangzhou 510275, China; 4. School of Geography and Tourism, Jiaying University, Meizhou 514015, China*)

Abstract: The TMS5e sequence from the Tumen section, at the southern edge of Tengger Desert in the northwestern China, is synchronous with Marine Isotope Stage 5e (MIS5e). It consists of 16 layers of aeolian dune sands, 11 layers of lacustrine loess-like facies, and 5 layers of lacustrine facies. The results of grain-size analysis shows that the palaeo-mobile dune sands, palaeo-fixed to semi-fixed dune sands and loess-like sandy loams are mainly composed of sands, ranging from 70% to 96%; their silt contents ranged from 4% to 20%, and their clay contents ranged from 1% to 5%; the climate under which the aeolian dune sands were deposited is similar to that under which modern mobile dune sands form, which is caused by the dominance of the cold, dry East Asian winter monsoon. In contrast, the lacustrine loess-like facies and lacustrine facies had a lower sand contents than those of the three aeolian dune sands, but have higher silt and clay contents, most of their sand content ranged from 30% to 60%, their silt contents ranged from 35% to 55%, and their clay contents ranged from 6% to 20%. The lacustrine loess-like facies and lacustrine facies formed under the influence of the warm, humid East Asian summer monsoon based on their similarity with modern sediments. The grain-size indicator Mz (mean grain diameter) and the SC/D value in the TMS5e sequence indicate climatic instability at the southern edge of the Tengger Desert during MIS5e, with at least 14 fluctuations between a warm, humid climate and a cold, dry climate, divided into five stages: TMS5e5 (139 kyr to 129.3 kyr B.P.), TMS5e4 (129.3 kyr to 124 kyr B.P.), TMS5e3 (124 kyr to 119.5 kyr B.P.), TMS5e2 (119.5 kyr to 116.5 kyr B.P.), and TMS5e1 (116.5 kyr to 113.7 kyr B.P.). These correspond roughly to MIS5e5, MIS5e4, MIS5e3, MIS5e2, and MIS5e1, respectively, in the GRIP ice core data.

Keywords: Tengger Desert; Tumen section; TMS5e sequence; grain-size characteristics; palaeoclimate reconstruction; Marine Isotope Stage 5e (MIS5e)

Citation: Wen Xiaohao, Li Baosheng, Wang Fengnian, Zheng Yanming, Niu Dongfeng, Si Yuejin, Ou Xianjiao, 2012. Grain-size characteristics and climate variability in TMS5e sequence of Tumen section in southern Tengger Desert, northwestern China. *Chinese Geographical Science*, 22(1): 48–62. doi: 10.1007/s11769-012-0513-5

1 Introduction

The degree of climate instability during Marine Isotope Stage 5e (MIS5e) has been disputed since the 1990s. In 1993, studies of oxygen isotopes and the chemical constituents in the ice core data of Greenland Ice Core Project (GRIP) discovered extreme millennial- to century-scale variability during MIS5e (Dansgaard *et al*., 1993; GRIP Members, 1993). However, a similar climate record from the ice core of Greenland Ice Sheet Project 2 (GISP2), located only 28 km from the GRIP site, failed to show these strong oscillations at the same

Received date: 2011-02-22; accepted date: 2011-10-10

Foundation item: Under the auspices of State Key Laboratory of Loess and Quaternary Geology, Institute of Earth Environment, Chinese Academy of Sciences (No. SKLLQG0901, SKLLQG1013), Research Fund for the Doctoral Program of Higher Education of China (No. 20094407120004)

Corresponding author: LI Baosheng. E-mail: Libsh@scnu.edu.cn

time (Grootes *et al.*, 1993; Taylor *et al.*, 1993). Since then, equally contradictory climatic records during MIS5e have been reported in European lake deposits, deep-sea drilling cores from the Nordic sea, Western Pacific, or northern Atlantic Ocean, and NGRIP ice cores from Greenland (Field *et al*., 1994; Thouveny *et al*., 1994; Fronval and Jansen, 1996; Linsley, 1996; Zagwijn, 1996; Adkins *et al*., 1997; Frogley *et al*., 1999; Rioual *et al*., 2001; NGRIP Members, 2004; Rousseau *et al*., 2006; Couchoud *et al*., 2009).

Similarly contradictory evidence for climate variability during MIS5e has been recorded in loess and lacustrine deposits in China. An and Porter (1997) reported that two dust peaks within MIS5e were correlated with cold events based on the quartz fraction > 40 μm. Guan *et al*. (1996) considered that MIS5e should be divided into three warm substages separated by two cool periods based on the $CaCO_3$ contents in S1 of the Beiyuan loess. Zhang *et al*. (1998) reconstructed three relatively warm and humid periods, with high lake levels, interrupted by two relatively cold and dry periods, with low lake levels, during MIS5e in the RM core from the Zoigê Basin of China's Qinghai-Tibet Plateau. However, Ren *et al*. (1996) and Liu *et al*. (1998) considered that the East Asian monsoon was very stable during MIS5e based on the results of grain size and magnetic susceptibility analyses in Chinese loess deposits. Guan *et al*. (2007) thought that the East Asian monsoon is instable, but MIS5e relatively stable in early Last Interglacial through the analysis of grain-size and the chemical elements in Shagou loess section on the southern edge of the Tengger Desert.

In recent years, we have studied the multi-cycle sedimentary sequence of aeolian dune sands and lacustrine deposits during periods synchronous with MIS5e. We have named this multi-cycle sedimentary sequence the ′TMS5e′ sequence. In the present paper, we discuss climate variability during MIS5e based on the results of our analysis of the grain-size distribution and chronology in the TMS5e sequence.

2 Materials and Methods

2.1 TMS5e sequence in Tumen section

The Tumen section (37°38′N, 103°09′E, 1730 m a.s.l.) is located near Tumen Village, in the northeastern part of the Gulang Oasis at the southern margin of the Tengger Desert in the northwestern China (Fig. 1). The site is north of the Qilian Mountains and lies at the intersection of the Qinghai-Tibet Plateau, the Mongolian Plateau, and the Loess Plateau. The Gulang chorography (Committees of Gulang County, 2000) indicates that the site is part of the semi-arid cold alpine region of the Qilian Mountains. The mean annual temperature is 4.9℃, with an average temperature of –9.8℃ during the coldest month (January) and an extreme minimum temperature of –26.4℃, and an average temperature of 17.5℃ during the hottest month (July) and an extreme maximum temperature of 33℃. The mean annual precipitation is 307 mm, of which 90% fall from April to October, and the annual evaporation is about 2800 mm. In winter, the climate is controlled by East Asian continental air masses, with prevailing northerly winds and frequent sandstorms at low altitudes, but with prevailing westerly winds at high altitudes; in summer, it is dominated by prevailing southerly winds under the influence of a subtropical high pressure zone in the West Pacific or the input of the warm and humid southwest monsoon from the Indian Ocean, which brings heavy rain and storms in some places.

The Tumen section is part of an outcrop that is 32 m thick. In this paper, we focused on the TMS5e sequence (Fig. 2a), which occupies the bottom part of the section at a depth from 27.76 m to 31.71 m and consists of 32 layers of sedimentary units, including 16 layers of aeolian dune sands, 11 layers of lacustrine loess-like facies, and 5 layers of lacustrine facies.

The aeolian dune sands are yellowish-brown (Munsell 10YR5/8), loose, well sorted, and contain some clear inclined or cross beddings. Based on differences in the grain-size distribution, the aeolian dune deposits can be divided into three types: palaeo-mobile dune sediments (D), which are mainly composed of fine sands; palaeo-fixed to semi-fixed dune sediments (FD), which primarily consist of silty very fine sands; and loess-like sandy loams (LD), which mainly contain silty to very fine sands. The lacustrine loess-like facies (GL) mostly contain brown-yellow (2.5YR4/2) silty very fine sands with well-developed horizontal bedding and current ripples. The lacustrine facies (LS) are made up of silty fine sands and are light grey-yellow (2.5YR6/2) or pale yellow (2.5YR8/4), showing well-developed horizontal bedding. These deposits suggest the presence of more than 14 sedimentary cycles in the TMS5e sequence,

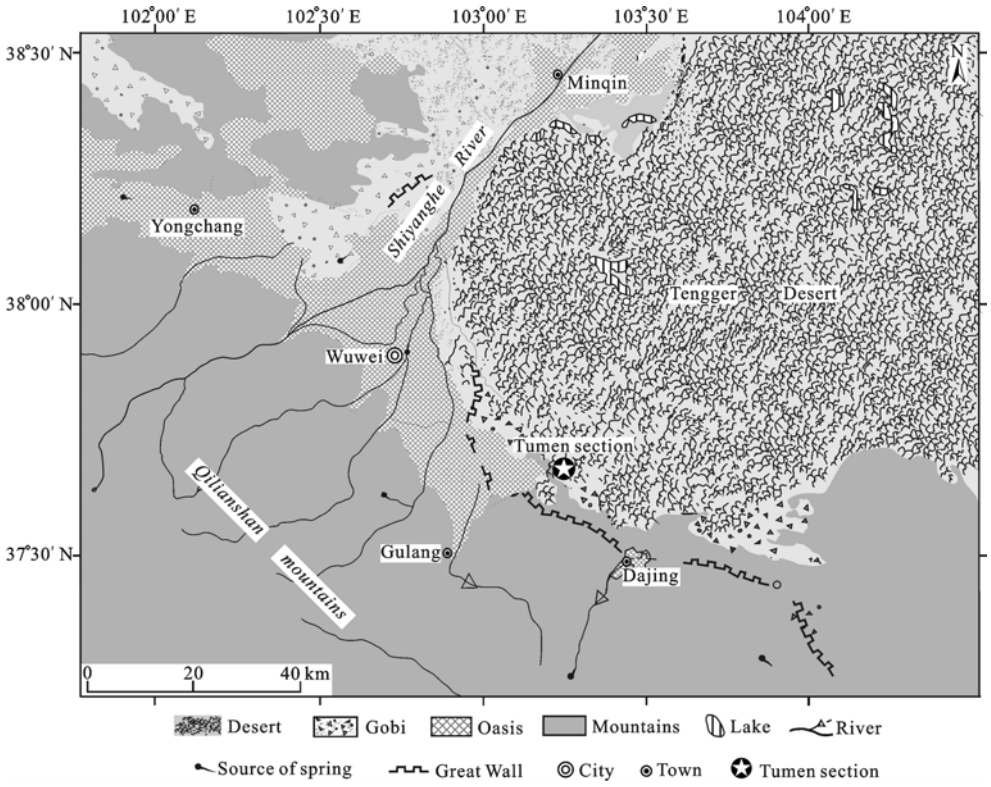

Fig. 1 Location of Tumen section in southern Tengger desert

which are composed of aeolian dune deposits alternating with lacustrine deposits or lacustrine loess-like facies.

2.2 Experimental methods

We obtained samples for thermoluminescence (TL) dating from the uppermost, middle, and bottom parts of TMS5e (Fig. 2a). We used the multiple-aliquot technique for the fine-grained quartz fraction with particles ranging from 2 μm to 8 μm in diameter, following the method of Aitken (1998). These samples were analyzed at the Guangzhou Institute of Geochemistry, Chinese Academy of Sciences, using TL dating instruments (models 711 and 7185) made by Littlemore Scientific Co. (Oxford, UK). Table 1 provides the detailed dating parameters.

Sampling provided 182 samples obtained at intervals of 2 cm. Careful chemical pretreatment and analysis were conducted following the guidelines of Konert and Vandenberghe (1997), including the following procedures: First, we dried all samples at temperature below 40℃, and then placed 0.5 g to 1.0 g of each sample into a 1000-mL breaker. We removed organic matter and carbonates by boiling with 30% hydrogen peroxide and enough hydrochloric acid for about 20 minutes. We removed the dissolved cations using deionized water. After shaking the residues in 100 mL of sodium hexametaphosphate (0.05 mol/L) solution for 10 minutes, we left the solution to stand overnight, then decanted the clear water from the samples in the morning. Finally, we analyzed all pre-treated samples to determine their grain-size distribution at the School of Geography, South China Normal University, Guangzhou, China, using a Mastersizer 2000M analyzer (Malvern Instruments, Malvern, U.K.), which has a measurement range of 0.02 μm to 2000 μm. We repeated the determination three times for each sample, and used the average value in subsequent analyses. All grain-size data were stored in a database and the values of various parameters were calculated by using the MatLab 7.0 software. We subdivided the samples into 101 grain-size grades (including sizes of 2.0 mm to 0.1 mm and < 0.1 mm) following the general principles in the Chinese classification standard for loess deposits (Liu, 1985); all other size ranges were the standard set provided by the instrument.

We expressed the grain size as ϕ, with $\phi = -\log_2 d$ (Krumbein and Pettijohn, 1938), where d is the diameter of the particle (mm). We also calculated several descriptive statistics, including the mean diameter (Mz), standard deviation (σ), skewness (Sk), and kurtosis (Kg), using the following equations proposed by Folk and Ward (1957):

$$Mz = (\phi 16 + \phi 50 + \phi 84) / 3$$

$$\sigma = [(\phi 84 - \phi 16) / 4] + [(\phi 95 - \phi 5) / 6.6]$$

$$Kg = (\phi 95 - \phi 5) / [2.44(\phi 75 - \phi 25)]$$

$$Sk = \{(\phi 84 + \phi 16 - 2\phi 50) / [2(\phi 84 - \phi 16)]\} + \{(\phi 95 + \phi 5 - 2\phi 50) / [2(\phi 95 - \phi 5)]\}$$

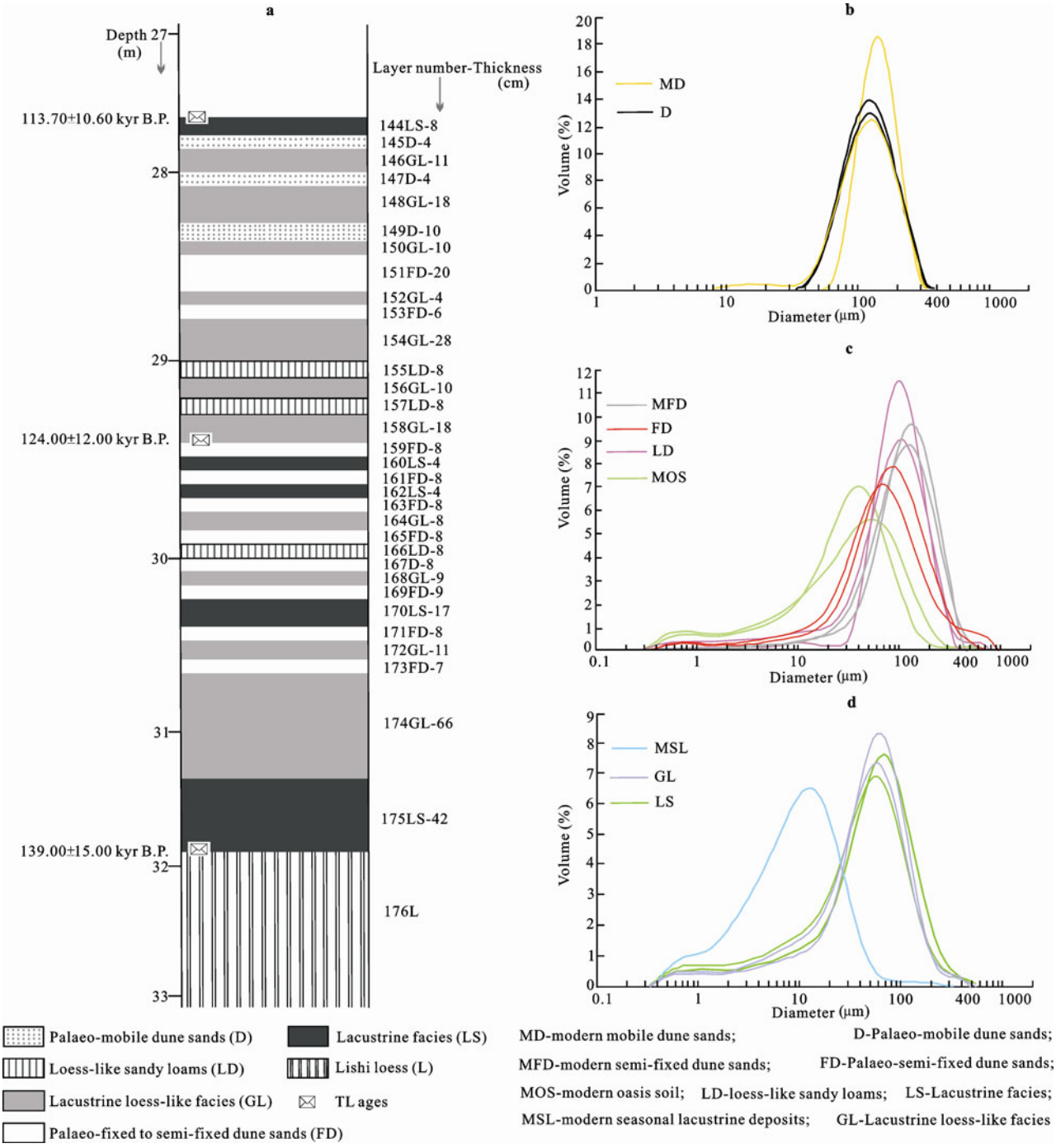

Fig. 2 TMS5e sequence (a) and frequency curves for grain-size distribution (b, c, d) in different sedimentary facies

3 Results and Analyses

3.1 Chronology

The TL dating results for the TMS5e sequence (Table 1, Fig. 2a) show a TL age of 113.70 ± 10.60 kyr B.P. for the upper part of the sequence and 139.00 ± 15.00 kyr B.P. for the bottom part. The top of the TMS5e sequence therefore corresponds to the age of the boundary between MIS5d and MIS5e (114 kyr B.P.) in the SPECMAP curves (Martinson *et al*., 1987). The age at the bottom is approximately equivalent to the age of 140 ± 10 kyr B.P. from the bottom of palaeosol S1 in the Shagou section (Guan *et al*., 2007). Considering these dates and the TL dating error of ± 10 kyr to 15 kyr B. P., the age of the TMS5e sequence appears to correspond to that of MIS5e. The three TL ages (y) were strongly and significantly correlated with the depth (x):

$$y = 6.4153x + 64.541 \quad (R^2 = 0.993, p < 0.05)$$

This indicates that the dating was reliable. Thus, we have dated all other layers using this regression equation to determine sedimentation rates. This method would certainly lead to age estimation errors, but it provides a satisfactory method for roughly understanding the millennial-scale or longer environmental and climatic changes that occurred during MIS5e in the study area.

3.2 Grain-size characteristics

3.2.1 Grain-size distribution in sedimentary facies

Table 2 presents the overall grain-size distribution of the various sedimentary facies, and Fig. 2 and Fig. 3 present this data in graphical form. The 12 samples of palaeo-mobile dune sands show a unimodal frequency distribution (Fig. 2b) and have a high sand content, ranging from 93.16% to 100%, with an average of 96.88%. The fine sands accounted for the highest proportion of the total, followed by very fine sands and medium sands; coarse sands and the silt and clay component (< 0.005 mm) were present at very low levels, and were sometimes even entirely absent (Fig. 3).

The 28 samples of palaeo-fixed to semi-fixed dune sands had a weakly bimodal frequency distribution (Fig. 2c), with one significant peak for fine or very fine sands and a weak peak for silt. The overall sand content averaged 84.66%, with values ranging from 69.49% to 92.46%, and was dominated by fine or very fine sands, followed by medium sands. Compared with the palaeo-mobile dune sands, there were higher percentages of silts and clays, ranging from 6.89% to 23.45% and from 0.45% to 7.06%, respectively, with averages of 12.83% and 2.54%, respectively.

The 12 samples of loess-like sandy loams also had a weakly bimodal frequency distribution (Fig. 2c), similar to the results for the palaeo-fixed to semi-fixed dune sands. The sand contents ranged from 62.63% to 75.68%, with an average of 70.18%; the percentages of very coarse, coarse, and medium sands were generally less than 15%. The silt and clay contents were much higher than those in the palaeo-fixed to semi-fixed dune sands, with values ranging from 19.78% to 31.65% and from 3.19% to 5.72%, respectively, with averages of 25.69% and 4.13%, respectively.

The 37 samples of lacustrine facies and 93 samples of lacustrine loess-like facies had clearer bimodal frequency distribution (Fig. 2d). There was one significant peak for very fine sands or coarse silt, with a weaker peak for fine silt or clay. The sand contents of all samples from the lacustrine and lacustrine loess-like facies ranged from 19.94% to 67.98% and from 24.37% to 65.22%, respectively, with averages of 48.22% and 45.93%, respectively. The silt contents ranged from 25.56% to 56.13% and from 28.13% to 58.66%, respectively, with averages of 40.99% and 43.69%, respectively. The clay contents ranged from 5.76% to 23.93% and from 5.79% to 18.86%, respectively, with averages of 10.79% and 10.38%, respectively. The dominant fractions were silt or very fine sand, followed by fine sands and clay; very coarse, coarse, and medium sands

Table 1 TL ages at three depths in TMS5e sequence and associated analytical data

Horizon (laboratory number)	Depth (m)	U (ppm)	Th (ppm)	K (%)	Total activity (Gy)	Annual activity (mGy)	TL ages (kyr B.P.)
TL23 (TGD818)	27.76	0.52 ± 0.03	22.87 ± 0.46	1.91 ± 0.015	510.00 ± 40.80	4.50 ± 0.16	113.70 ± 10.60
TL25 (TGD819)	29.43	0.21 ± 0.01	21.59 ± 0.43	1.86 ± 0.015	571.20 ± 51.40	4.61 ± 0.14	124.00 ± 12.00
TL27 (TGD798)	31.71	1.31 ± 0.07	16.39 ± 0.33	2.22 ± 0.018	554.80 ± 41.66	3.99 ± 0.12	139.00 ± 15.00

Note: TGD, Guangzhou Institute of Geochemistry, Chinese Academy of Sciences

Table 2 Comparison of grain-size distribution in sedimentary facies from southern edge of Tengger Desert

		Proportion in each grain-size class (%)							
		VCS	CS	MS	FS	VFS	CFS	FFS	CL
TMS5e facies									
D (12)	Range	0	0–0.16	2.23–26.69	50.01–68.74	4.57–41.95	0–0.55	0–0.73	0–0.95
	Average	0	0.01	10.78	60.26	25.82	2.58	0.27	0.28
FD (28)	Range	0–0.15	0–1.06	0.09–8.27	32.79–55.72	29.63–46.03	6.07–20.79	0.53–4.08	0.45–7.06
	Average	0.01	0.08	2.66	43.16	38.73	11.40	1.43	2.54
LD (12)	Range	0–10.92	0–15.09	3.45–10.77	19.63–41.48	20.86–34.20	17.27–28.52	1.96–3.13	3.19–5.72
	Average	2.36	4.29	6.50	27.99	29.04	23.36	2.34	4.13
GL (93)	Range	0–0.22	0–2.06	0–4.22	5.55–29.42	16.56–40.38	24.10–49.71	3.16–12.37	5.79–18.86
	Average	0.01	0.19	0.83	14.83	29.92	37.90	5.92	10.40
LS (37)	Range	0	0–0.44	0–5.01	5.90–34.64	14.03–35.53	21.98–44.90	3.41–15.41	5.76–23.93
	Average	0	0.12	1.23	17.39	29.48	35.04	5.95	10.79
Modern deposits									
MD (83)	Range	0	0–1.77	0–41.60	53.59–83.04	1.47–40.18	05.77	0–1.66	0–2.90
	Average	0	0.08	17.60	67.00	12.97	1.74	0.24	0.37
MFD (27)	Range	0	0–3.19	0–16.33	39.13–57.86	17.26–44.27	6.51–13.26	0.81–2.67	0.85–5.81
	Average	0	0.32	8.57	49.25	27.67	9.83	1.57	2.79
MOS (5)	Range	0	0–0.61	0.64–1.76	12.40–28.59	23.76–34.34	25.84–41.68	3.02–8.30	4.90–13.79
	Average	0	0.11	1.22	21.47	29.36	32.25	5.69	9.89
MSL (5)	Range	0	0–0.07	0–0.53	0.27–0.70	0.62–1.37	32.90–45.87	23.84–26.55	28.16–40.32
	Average	0.00	0.03	0.28	0.47	0.94	39.00	25.06	34.21

Notes: D, palaeo-mobile dune sands; FD, palaeo-fixed to semi-fixed dune sands; LD, loess-like sandy loams; GL, lacustrine loess-like facies; LS, lacustrine facies; MD, modern mobile dune sands; MFD, modern semi-fixed to fixed dune sands; MOS, modern oasis soils; MSL, modern seasonal lacustrine deposits; VCS, very coarse sands (2000 μm to 1000 μm); CS, coarse sands (1000 μm to 500 μm); MS, medium sands (500 μm to 250 μm); FS, fine sands (250 μm to 100 μm); VFS, very fine sands (100 μm to 50 μm); CFS, coarse silts (50 μm to 10 μm); FFS, fine silts (10 μm to 5 μm); CL, clays (< 5 μm)

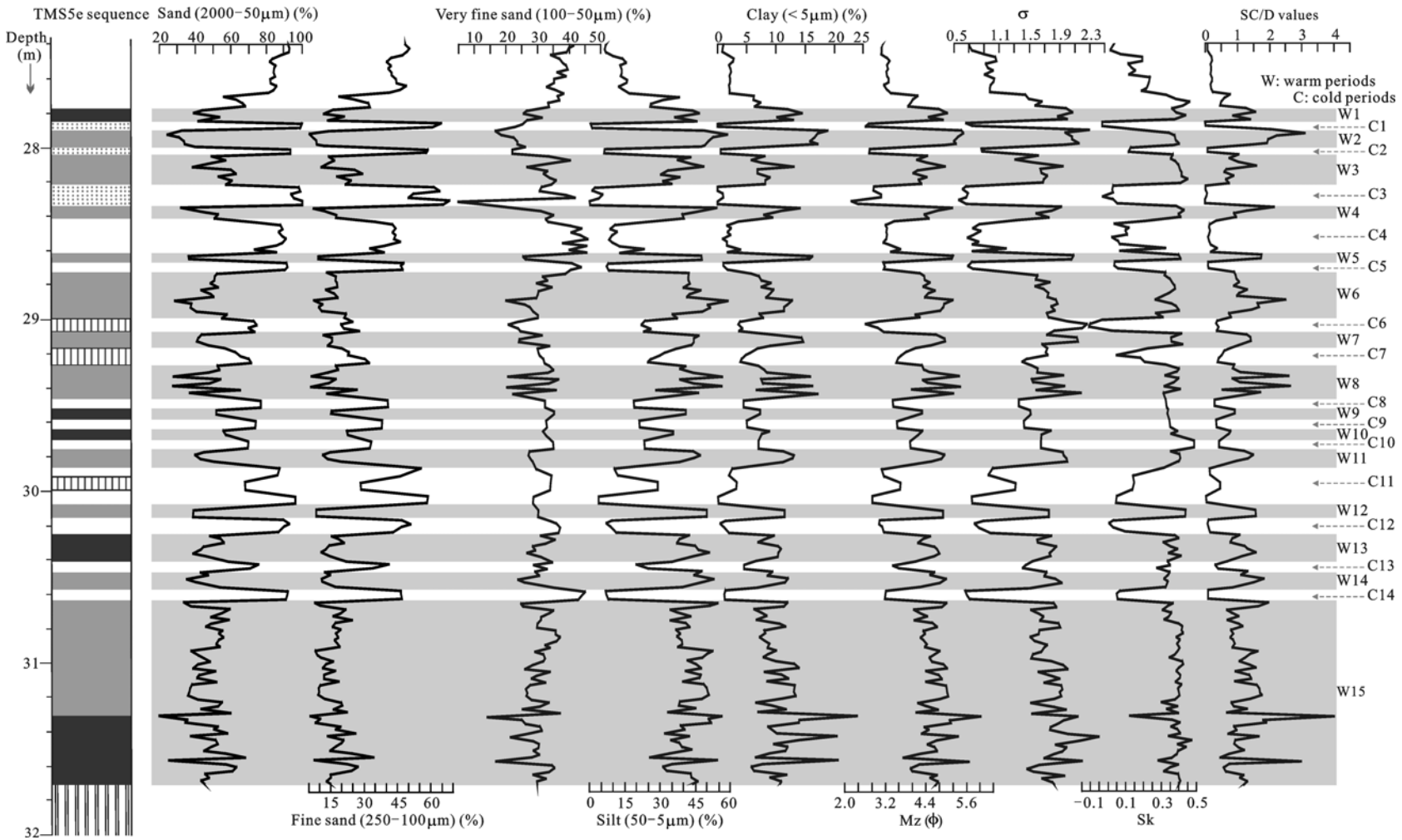

Fig. 3 Fluctuations in grain-size distribution and related statistical parameters within TMS5e sequence of Tumen section

were present at low levels or were entirely absent.

3.2.2 Grain-size parameters of sedimentary facies

Table 3 summarizes the grain-size parameters of the sedimentary facies in the TMS5e sequence, and Fig. 4 presents the relationships between these parameters visually. The grain-size distribution and sorting of the sedimentary facies can be judged from the mean diameter (Mz) and its standard deviation (σ): palaeo-mobile dune sands have values of these parameters that confirm the high abundance of fine sands and indicate well-sorted to very well-sorted deposits; the palaeo-fixed to semi-fixed dune sands and loess-like sandy loams have values of these parameters that correspond to fine to very fine sands, indicating moderately to well-sorted and poorly to badly sorted deposits, respectively; and the lacustrine and lacustrine loess-like facies have values of these parameters that correspond to very fine sands to coarse silts, indicating poorly sorted to unsorted deposits.

The skewness (Sk) and kurtosis (Kg) values suggest that the palaeo-mobile dune sands have nearly symmetrical peaks, with moderate kurtosis. These parameters for the palaeo-fixed to semi-fixed dune sands and the loess-like sandy loams suggest nearly symmetrical to positively skewed peaks with medium to sharp kurtosis, whereas the lacustrine and lacustrine loess-like facies also show positively skewed peaks and medium to sharp kurtosis. Both the average and range of SC/D (SC/D is the ratio of the summation of silt and clay to sands) increase moving from the palaeo-mobile dune sands to the palaeo-fixed to semi-fixed dune sands, and from these sands to the loess-like sandy loams or lacustrine facies.

To further distinguish among the various sedimentary facies, we prepared scatterplots of Mz versus σ, Sk, Kg, and SC/D using data from the 182 samples (Fig. 4). These diagrams show that the samples of palaeo-mobile dune sands and palaeo-fixed to semi-fixed dune sands are closely clustered, with values of Mz ranging from 2.20ϕ to 3.40ϕ, values of σ ranging from 0.50 to 1.00, values of Sk ranging from –0.05 to 0.15, and values of SC/D ranging from 0 to 0.10. The ranges for the lacustrine and lacustrine loess-like facies appear to overlap,

Table 3 Comparison of grain-size parameters between sedimentary facies at southern edge of Tengger Desert

Types		Mz (ϕ)	σ	Sk	Kg	SC/D values
TMS5e facies						
D (12)	Range	2.21–3.09	0.56–0.87	–0.03–0.13	0.92–1.15	0–0.07
	Average	2.74	0.70	0.03	0.99	0.03
FD (28)	Range	3.03–3.95	0.65–1.65	0–0.49	0.93–1.63	0.08–0.44
	Average	3.31	0.97	0.15	1.22	0.19
LD (12)	Range	2.62–3.81	1.31–2.26	–0.11–0.35	0.87–1.59	0.32–0.60
	Average	3.39	1.68	0.11	1.31	0.43
GL (93)	Range	3.99–5.52	1.29–2.29	0.12–0.45	0.94–1.56	0.53–3.10
	Average	4.65	1.77	0.37	1.32	1.28
LS (37)	Range	3.74–6.03	1.46–2.42	0.12–0.47	0.96–1.57	0.47–4.02
	Average	4.60	1.83	0.37	1.31	1.20
Modern deposits						
MD (83)	Range	2.02–3.18	0.46–1.44	–0.07–0.40	0.882.07	0–0.08
	Average	2.48	0.68	0.09	1.05	0.02
MFD (27)	Range	1.95–3.42	0.61–1.44	0.03–0.40	0.94–2.08	0.11–0.22
	Average	2.96	1.10	0.25	1.44	0.17
MOS (5)	Range	3.97–5.03	1.41–2.12	0.25–2.42	1.04–1.41	0.56–1.70
	Average	4.47	1.85	0.38	1.26	0.97
MSL (5)	Range	6.71–7.22	1.51–1.58	0.11–0.21	0.99–1.06	45.73–111.38
	Average	6.97	1.53	0.18	1.03	63.19

Notes: D, palaeo-mobile dune sands; FD, palaeo-fixed to semi-fixed dune sands; LD, loess-like sandy loams; GL, lacustrine loess-like facies; LS, lacustrine facies; MD, modern mobile dune sands; MFD, modern semi-fixed to fixed dune sands; MOS, modern oasis soils; MSL modern seasonal lacustrine deposits

with values of Mz ranging from 4.00ϕ to 5.60ϕ, values of σ ranging from 1.50 to 2.30, values of Sk ranging from 0.25 to 0.45, and values of SC/D ranging from 0.60 to 3.20. The boundaries between the two former and two latter groups are fairly distinct. The parameters for the loess-like sandy loams fall between the two former and two latter groups, with values of Mz ranging from 2.80ϕ to 3.80ϕ, values of σ ranging from 1.40 to 2.20, values of Sk ranging from –0.10 to 0.20, and values of SC/D ranging from 0.35 to 0.50.

The results of our regressions for the scatterplots in Fig. 4 show different strengths of the relationship between Mz and the other parameters. The correlation coefficients (R^2) for the Mz-σ, Mz-SC/D, and Mz-Sk relationships were 0.695, 0.834 and 0.568, respectively (all $p < 0.05$). That is, the values of σ, Sk, and SC/D all increased with increasing Mz. These correlations indicate good relationships between Mz and these parameters and provide clues to when the depositional processes change from blowing sands to lacustrine processes as the wind's strength decreases. To understand these relationships, it is necessary to account for the grain-size eigenvalues of ϕ95 and ϕ84, which represent the content changes for fine silts and clay, respectively. In Table 2, both fine silts and clay have no contribution to the ϕ95 eigenvalue for aeolian dune sands, and only slightly influence the ϕ95 eigenvalue for the loess-like sandy loams, but both strongly affect the ϕ95 and ϕ84 eigenvalues for lacustrine and lacustrine loess-like facies. Though the SC/D values have no direct physical relationship to the grain-size eigenvalues, they were nonetheless significantly correlated with these eigenvalues.

The scatterplot for Mz versus Kg (Fig. 4c) shows no overall order in the positions of the various sedimentary facies, lacking distinctive locations and boundaries and showing no significant correlation: the Kg values of

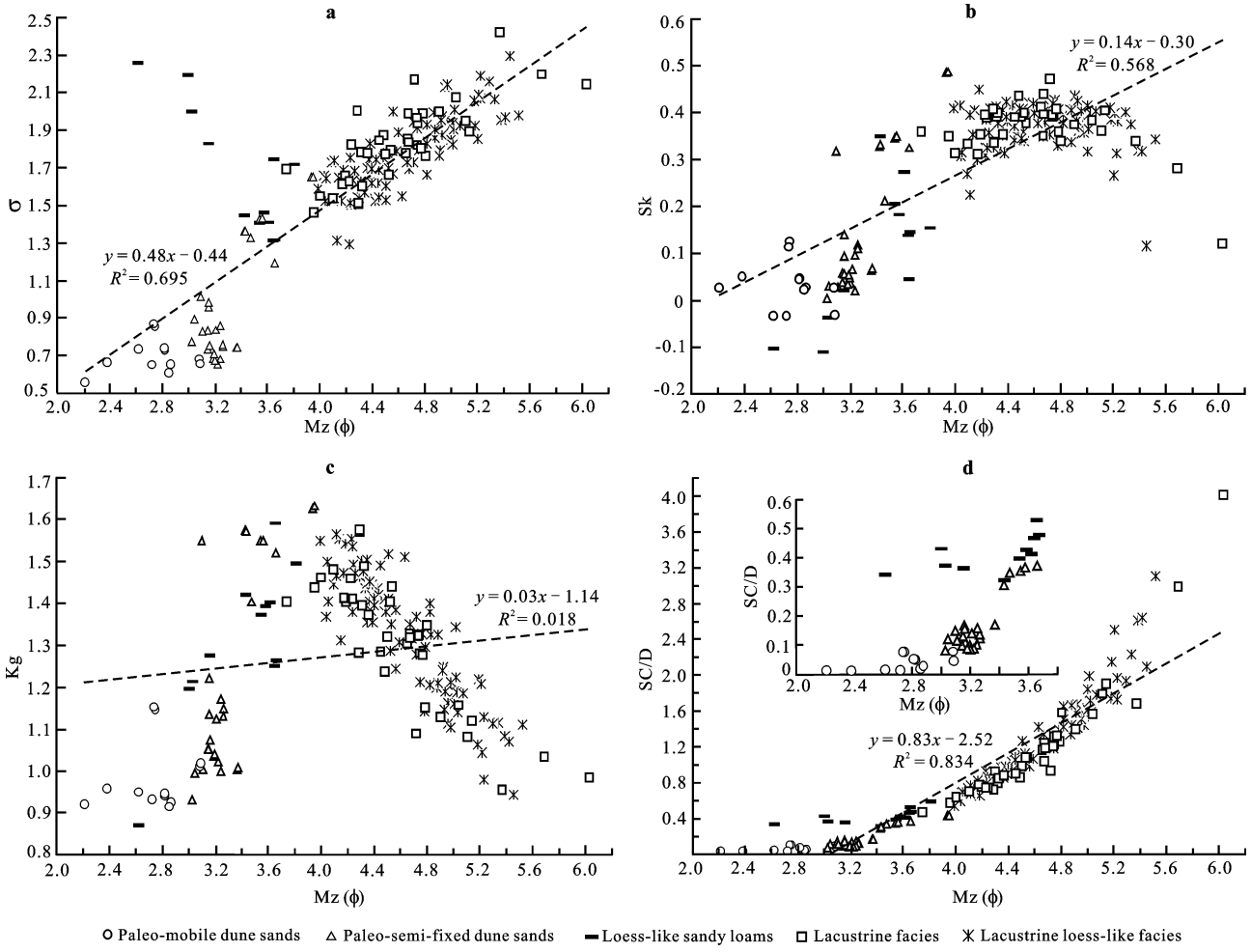

Fig. 4 Scatterplots of Mz versus σ, Sk, Kg, and SC/D in different sedimentary facies of TMS5e sequence

palaeo-mobile dune sands and palaeo-fixed to semi-fixed dune sands ranged from 0.90 to 1.20, those of the loess-like sandy loams ranged from 1.20 to 1.60, and those of the lacustrine and lacustrine loess-like facies ranged from 1.00 to 1.60. The characteristics of the Mz versus Kg relationship embody the fact that the values of Kg are essentially only correlated with the grain-size distribution. Based on the statistics for the four eigenvalues from the formula we used to calculate Kg , 80% of the samples from palaeo-mobile dune sands, palaeo-fixed to semi-fixed dune sands, loess-like sandy loams, lacustrine facies, and lacustrine loess-like facies have the following ranges for ϕ95 to ϕ5: 1.98 to 2.41, 2.23 to 6.08, 5.25 to 7.25, 5.80 to 6.90, and 6.08 to 6.89, respectively. The corresponding values for ϕ75 to ϕ25 range from 0.81 to 1.04, 0.88 to 1.53, 1.55 to 2.66, 1.58 to 2.48, and 1.77 to 2.36, respectively. Therefore, most samples from palaeo-mobile dune sands have lower ϕ95 to ϕ5 and ϕ75 to ϕ25 values than those of the loess-like sandy loams, lacustrine facies, and lacustrine loess-like facies; the values for the latter three groups tend to be close. The values for the palaeo-fixed to semi-fixed dune sands fall between the former and latter groups. Because of these relationships, we will not discuss Kg further in the remainder of the text.

3.2.3 Fluctuations in grain-size distribution and relative parameters

Figure 3 illustrates the evolution of the grain-size distribution and related statistical parameters as a function of depth in the TMS5e sequence. The results show the striking variations between high and low values throughout the sequence. The grain-size distribution and parameters clearly differ among the various sedimentary facies. For example, the contents of sands, fine sands, and very fine sands increase in the facies that comprise palaeo-mobile dune sands, palaeo-fixed to semi-fixed dune sands, and loess-like sandy loams, whereas the contents of silts and clays and the values of Mz, σ, Sk, and SC/D tend to decrease in these facies. The lacustrine and lacustrine loess-like facies show the opposite trend, with the contents of silts and clays and the values of Mz, σ, Sk, and SC/D increasing. Therefore, moving vertically within the TMS5e sequence, the fluctuations in the proportions of the three sand categories (sands, fine sands and very fine sands) and of the six other categories (silt, clay, Mz, σ, Sk, and SC/D) represent mirror images. Our results suggest at least 14 grain-size cycles, which we believe represent distinct deposition cycles.

4 Discussion

4.1 Palaeoclimate and environmental conditions indicated by grain size characteristics in different facies

The Tengger Desert is located in the margin of the monsoonal region of the northwestern China and has been sensitive to fluctuations in the East Asian monsoons since the late Quaternary, and the same situation exists for the Mu Us and Badain Juran deserts (Gao *et al*., 1993). The TMS5e sequence maybe therefore represent a true geological record dominated by the East Asian monsoon. According to our understanding of the evolution of the monsoonal environment of the eastern desert regions of China, the grain-size fluctuations between distribution dominated by coarse particles and the evenness of the distribution provide important clues about variations in the East Asian monsoons (Li *et al*., 2000; Qiang *et al*., 2004; Wen *et al*., 2009; Lu *et al*., 2010). Based on the conclusions of previous research, the aeolian sandy materials (including the palaeo-mobile dune sands, palaeo-fixed to semi-fixed dune sands, and loess-like sandy loams) were products of the prevailing palaeo-East Asian winter monsoon. On this basis, we can hypothesize that during the time period covered by the TMS5e sequence, the Siberia-Mongolia high-pressure cell led to southward air movements in the northern hemisphere, and a cold, dry, and windy climate occurred repeatedly in the Tengger Desert. Under these climatic and environmental conditions, biochemical weathering (including pedogenesis) would have been weak and the physical processes of erosion, followed by sediment transport and accumulation, would have prevailed. Finer, lighter, more easily transported fractions would be continuously blown away, whereas coarser and heavier quartz sands that are more resistant to weathering, mainly containing particles < 4.32ϕ, would be retained to form aeolian mobile dunes (Li *et al*., 2000; Wen *et al*., 2009). As a result, the mean particle size would became coarser, showing a well-sorted and relatively concentrated grain-size distribution, as well as decreasing SC/D values.

Despite the importance of the palaeo-East Asian winter monsoon, the East Asian summer monsoon would also occasionally increase in strength, extending to-

wards the north and west and penetrating into the study area, bringing higher seasonal rainfall. As a result, vegetation such as grasses, shrubs, and even trees would grow better on the palaeo-mobile dune sands, leading to increasing fixation of the dune sands. The vegetation would eventually create a ′barrier′ that stabilizes the soil, and that may collect and even generate finer particles such as silts and clays; these dust particles improve water retention and help vegetation grow, leading to the evolution of the palaeo-fixed and semi-fixed sand dunes. Consequently, these dunes would have higher contents of grains > 4.32ϕ than the palaeo-mobile dune sands, and the values of σ, Sk, and SC/D would change accordingly.

If the palaeo-East Asian summer monsoon strengthened and invaded the study area during some periods, it would bring more rainfall and warmer temperature, causing the vegetation cover to increase, with oasis landscapes appearing. Even in winter and spring, the times of year with frequent dust storms, the vegetation barrier created by these oases would both block the invasion of coarse sands and provide a good place for the accumulation of fine dust, possibly even leading to the development of silts and clays. Subsequently, the loess-like sandy loams would form under the pedogenesis promoted by the oasis environment and the warmer temperature. Thus, the loess-like sandy loams have much higher contents of grains > 4.32ϕ than in the palaeo-mobile dune sands and the palaeo-fixed to semi-fixed dune sands, with moderately to well-sorted grains and positively skewed peak fractions, as well as increasing of SC/D values.

If the Siberia-Mongolia high pressure cell weakened and retreated northwards for a long period, the weakened palaeo-East Asian winter monsoon would be replaced by a progressively strengthened, northward-moving palaeo-East Asian summer monsoon, which would result in increasing precipitation and rising temperature (Li *et al.*, 2000; Wen *et al*., 2009). The higher precipitation and temperature would intensify biochemical weathering. Under these less harsh conditions, vegetation cover would increase and the formerly fixed dune sands might exhibit enhanced pedogenesis. Furthermore, the accumulation of coarser windblown sands would be replaced by the natural deposition of finer particles. Simultaneously, the more abundant precipitation would enter the southern Tengger Desert and infiltrate low- lying areas and the depressions between dunes, forming seasonal or perennial wetlands (Li *et al*., 2000). If seasonal dust storms of short duration happened frequently, more and finer particles (silts and clay) would invade the lakes and become lacustrine and lacustrine loess-like facies.

Figure 2, Table 2 and Table 3 compare the grain-size distribution and related parameters of the different sedimentary facies in the TMS5e sequence with those of modern sedimentary facies (including 83 samples of modern mobile dune sands, 27 samples of modern semi-fixed to fixed dune sands, 5 samples of modern oasis soils, and 5 samples of modern seasonal lacustrine deposits) from the southern edge of the Tengger Desert. Our results show that the grain-size characteristics of the palaeo-mobile dune sands in the TMS5e sequence resemble those of modern mobile dune sands. Similarly, the grain-size characteristics of the palaeo-fixed to semi-fixed sand dunes and loess-like sandy loams resemble those of modern semi-fixed to fixed dune sands and modern oasis soils, respectively. The grain-size characteristics of the lacustrine and lacustrine loess-like facies also resemble those of modern seasonal lacustrine deposits. These similarities confirm and deepen our understanding of the climate and environment during the geological time period covered by the TMS5e sequence.

We can conclude from this evidence that the aeolian dune sands (including palaeo-mobile dune sands, palaeo-fixed to semi-fixed sand dunes, and loess-like sandy loams) were products of cool, dry climate in which deserts expanded during a period when the palaeo-East Asian winter monsoon was the dominant force, whereas the lacustrine facies and lacustrine loess-like facies were deposited or formed during warmer, wetter periods dominated by the palaeo-East Asian summer monsoon, when deserts retreated. The facies in the TMS5e sequence suggest that at least 14 changes in the sedimentary environment were recorded in the sequence from lacustrine deposits to aeolian dune sands, and that these alternations reflect changes in the relative dominance of the palaeo-East Asian summer and winter monsoons.

4.2 Climatic variability during MIS5e in southern Tengger Desert

The trends in the nine palaeoclimatic proxies (Fig. 4), including the contents of sands, fine sands, very fine sands, silts, and clays, and the associated statistical pa-

rameters (Mz, σ, Sk, and SC/D), could be classified into two groups: groups with similar and different trends. For simplicity, we selected the Mz value and the SC/D ratio to reconstruct the palaeoclimate during the MIS5e period; the results using other parameters are similar. Increases in Mz and SC/D indicate a strengthening of the summer monsoon and a weakening of the winter monsoon, whereas decreases in Mz and SC/D indicate weakening of the summer monsoon and strengthening of the winter monsoon. That is, higher values of Mz and SC/D correspond to a warmer and more humid climate dominated by a strengthened palaeo-East Asian summer monsoon, abbreviated here as a ′warm period′ (W event in Fig. 5 and Table 4); in contrast, lower values of Mz and SC/D correspond to a colder and drier climate dominated by a strengthened palaeo-East Asian winter monsoon, abbreviated here as ′cold periods′ (C event in Fig. 5 and Table 4). According to the timescale developed in this study, we propose that 15 W events occurred alternating with a total of 14 C events occurred during the same period.

The duration of domination by the palaeo-East Asian summer monsoon totaled about 17 kyr, and the duration of domination by the palaeo-East Asian winter monsoon totaled 8.30 kyr. The duration of the C and W events mostly ranged from 0.50 kyr to 1.20 kyr, with a maximum of 7.10 kyr and a minimum of 0.20 kyr. In terms of the frequencies and durations of the oscillations between the palaeo-East Asian summer monsoon and the palaeo-East Asian winter monsoon, the TMS5e climate can be divided into five substages (Fig. 5):

(1) TMS5e5 (139 kyr to 129.3 kyr B.P.), corresponding to strata 175LS to 170LS, was composed of three W events (W15 to W13) totaling 8.9 kyr and two C events (C14 and C13) totaling 0.8 kyr. The values of Mz and SC/D from 80% of the samples ranged from 4.23ϕ to 6.03ϕ and 0.78 to 4.02, respectively, with averages of 4.52ϕ and 1.14ϕ, respectively. Both Mz and SC/D mostly showpeaks overlapped by several valleys, indicating a warmer and more humid climate.

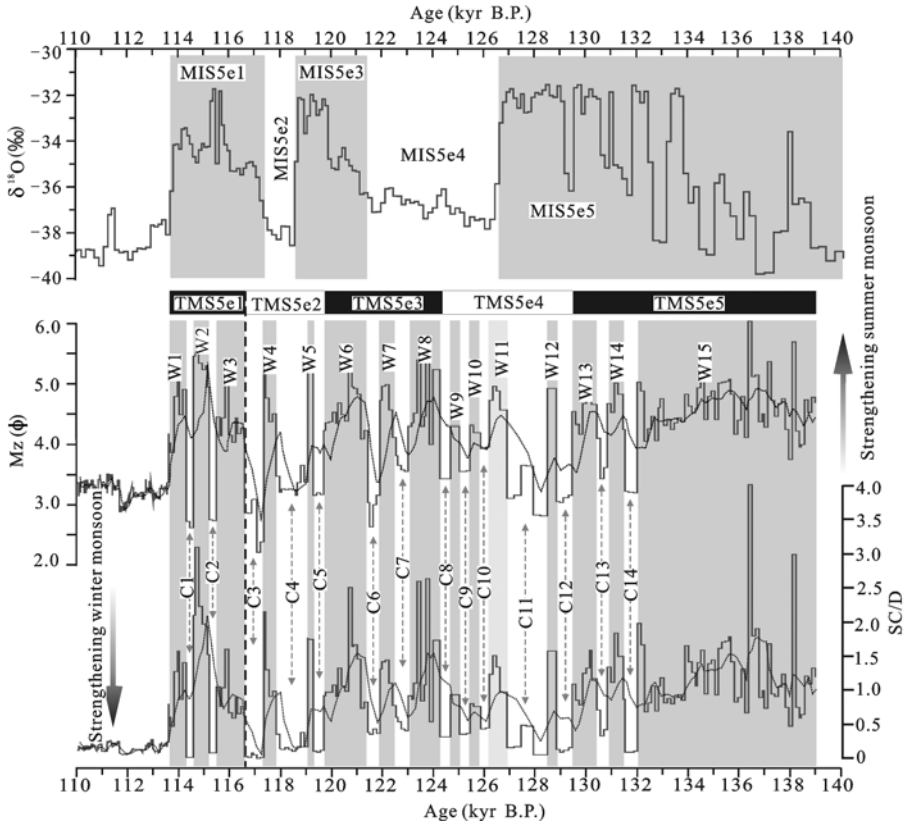

C: cold period; W: warm period

Fig. 5 Comparison of records for Mz and SC/D ratio in TMS5e sequence with $\delta^{18}O$ (‰) variations in GRIP ice core from Greenland (GRIP Members, 1993).

Table 4 Warm and cold periods indicated by grain-size proxy of Tumen section during MIS5e in southern Tengger desert

Warm period	Ages (kyr B.P.)	Duration (kyr)	Cold periods	Age (kyr B.P.)	Duration (kyr)
W1	113.70–114.20	0.5	C1	114.20–114.40	0.2
W2	114.40–115.10	0.7	C2	115.10–115.40	0.3
W3	115.40–116.50	1.1	C3	116.50–117.20	0.7
W4	117.20–117.70	0.5	C4	117.70–118.90	1.2
W5	118.90 –119.20	0.3	C5	119.20–119.60	0.4
W6	119.60–121.30	1.7	C6	121.30–121.80	0.5
W7	121.80–122.40	0.6	C7	122.40–122.90	0.5
W8	122.90–124.00	1.1	C8	124.00–124.50	0.5
W9	124.50–124.80	0.3	C9	124.80–125.30	0.5
W10	125.30–125.60	0.3	C10	125.60–126.10	0.5
W11	126.10–126.60	0.5	C11	126.60–128.20	1.6
W12	128.20–128.70	0.5	C12	128.70–129.30	0.6
W13	129.30–130.40	1.1	C13	130.40–130.70	0.3
W14	130.70–131.40	0.7	C14	131.40–131.90	0.5
W15	131.90–139.00	7.1			

(2) TMS5e4 (129.3 kyr to 124 kyr B.P.), corresponding to strata 169FD to 159FD, contained four W events (W12 to W9) totaling 1.6 kyr and five C events (C12 to C8) totaling 3.7 kyr. The values of Mz and SC/D from 80% of the samples ranged from 3.16ϕ to 4.96ϕ and 0.15 to 1.58, respectively, with averages of 3.82ϕ and 0.60, respectively. Both Mz and SC/D mostly showed valleys overlapped by some narrow peaks, indicating a relatively cold and dry climate.

(3) TMS5e3 (124 to 119.6 kyr B.P.), corresponding to strata 158GL to 152GL, included three W events (W8 to W6) totaling 3.4 kyr and two C events (C7 and C6) totaling 1.0 kyr. The values of Mz and SC/D from 80% of the samples ranged from 4.00ϕ to 5.42ϕ and 0.53 to 2.64, respectively, with averages of 4.52ϕ and 1.14, respectively. Mz and SC/D showed three peaks and two valleys, indicating a relatively warmer and more humid climate.

(4) TMS5e2 (119.6 kyr to 116.5 kyr B.P.), corresponding to strata 151FD to 149D, included two W events (W5 and W4) totaling 0.8 kyr and three C events (C5 to C3) totaling 2.3 kyr. The values of Mz and SC/D from 80% of the samples ranged from 3.08ϕ to 5.21ϕ and 0.05 to 2.15, respectively, with averages of 3.53ϕ and 0.44, respectively. Both Mz and SC/D mostly showed valleys overlapped by two narrow peaks, indicating a colder and drier climate.

(5) TMS5e1 (116.5 kyr to 113.7 kyr B.P.), corresponding to strata 148GL to 144LS, included three W events (W3 to W1) totaling 2.3 kyr and two C events (C2 and C1) totaling 0.5 kyr. The values of Mz and SC/D from 80% of the samples ranged from 4.18ϕ to 5.52ϕ and 0.75 to 3.10, respectively, with averages of 4.38ϕ and 1.13, respectively. Both Mz and SC/D predominantly showed three marked wide peaks and two narrow valleys, indicating a warmer and more humid climate.

In summary, the TMS5e climate revealed by the grain-size peaks and valleys in Fig. 5 was less stable, with more frequent oscillations, than the MIS5e climate recorded in the GRIP ice core (GRIP Members, 1993; NGRIP Members, 2004), deep-sea drillings in the North Atlantic (Adkins *et al*., 1997), and loess deposits in China (Guan *et al*., 1996; Ren *et al*., 1996; An and Porter, 1997; Liu *et al*., 1998). If we ignore the high age uncertainty of the TL dating in this paper, the patterns and amplitudes of variation within the millennial to ten-millennial timescale of the TMS5e climate in the southern Tengger Desert are roughly similar to other climate records from around the world, especially those of the $\delta^{18}O$ (‰) variations in the GRIP ice core from Greenland (GRIP Members, 1993). For instance, the relatively warmer TMS5e5, TMS5e3, and TMS5e1 periods appear to correspond to the marked $\delta^{18}O$ (‰) peaks of MIS5e5 (from 140 kyr to 127 kyr B.P.), MIS5e3 (from 122 kyr to 119 kyr B.P.), and MIS5e1 (from 117 kyr to 114 kyr B.P.), respectively. Similarly, the colder TMS5e4 and TMS5e2 periods correspond to

the lower $\delta^{18}O$ (‰) values during MIS5e4 (from 127 kyr to 122 kyr B.P.) and MIS5e2 (from 119 kyr to 117 kyr B.P.

In addition, there are tens of abrupt century- to millennial-scale climatic changes, similar to interstadial-stadial or Dansgaard-Oeschger oscillations during the last glacial of the GRIP ice core (GRIP Members, 1993) and in the data from the Hulu cave (Wang *et al*., 2001). As we noted earlier, the durations of the C and W events mostly ranged from 0.50 to 1.20 kyr, which is close to the periodicity of 1.45 kyr for ice-rafted debris events in the North Atlantic (Mayewski *et al*., 1997) and the 0.51 kyr periodicity of the North Atlantic thermohaline circulation (Stuiver and Braziunas, 1993). The unstable climate during TMS5e shown in the present paper suggests that the climate was closely related to the palaeo-East Asian monsoon system, which is controlled by the climate and circulation patterns in the northern hemisphere.

5 Conclusions

The TMS5e sequence from the Tumen section, at the southern edge of the Tengger Desert in the northwesten China consists of 16 layers of aeolian dune sands, 11 layers of lacustrine loess-like facies, and 5 layers of lacustrine facies. They constitute 14.5 grain-sedimentary cycles alternating the aeolian sands with overlying lacustrine facies or lacustrine loess-like facies in the vertical direction of the sequence.

The aeolian dune sands in the TMS5e sequence were similar to that under which modern mobile dune sands form, which is caused by the dominance of the cold, dry East Asian winter monsoon. However, the lacustrine loess-like facies and lacustrine facies formed under the influence of the warm, humid East Asian summer monsoon. The grain-size indicator Mz and the SC/D value in the TMS5e sequence indicate climatic instability at the southern edge of the Tengger Desert during MIS5e, alternating at least 14 times of cold, dry climate with 15 times of warm, humid climate, divided into five stages: TMS5e5 (139 kyr to 129.3 kyr B.P.), TMS5e4 (129.3 kyr to 124 kyr B.P.), TMS5e3 (124 kyr to 119.5 kyr B.P.), TMS5e2 (119.5 kyr to 116.5 kyr B.P.), and TMS5e1 (116.5 kyr to 113.7 kyr B.P.). These correspond roughly to MIS5e5, MIS5e4, MIS5e3, MIS 5e2, and MIS5e1, respectively, in the GRIP ice core data.

Acknowledgements

The authors thank Lu Liangcai and Wang Baolin (Guang zhou Institute of Geochemistry, Chinese Academy of Sciences) for their support in TL dating measuring.

References

Adkins J F, Boyle E A, Keigwin L *et al.*, 1997. Variability of the North Atlantic thermohaline circulation during the last interglacial period. *Nature*, 390(6656): 154–156. doi: 10.1038/36540

Aitken M J, 1998. *An Introduction to Optical Dating*. New York: Oxford Science Publications.

An Z S, Porter S C, 1997. Millennial-scale climatic oscillations during the Last Interglaciation in central China. *Geology*, 25(7): 603–606. doi: 10.1038/36540

Committees of Gulang County, 2000. *Gulang Chorography*. Lanzhou: Gansu Culture Press, 45–142. (in Chinese)

Couchoud I, Genty D, Hoffmann D *et al.*, 2009. Millennial-scale climate variability during the Last Interglacial recorded in a speleothem from south-western France. *Quaternary Science Reviews*, 28(27–28): 3263–3274. doi: 10.1016/j.quascirev.2009.08.014

Dansgaard W, Johnsen S J, Clausen H B *et al.*, 1993. Evidence for general instability of past climate from a 250-kyr ice-core record. *Nature*, 364(6434): 218–220. doi: 10.1038/364218a0

Field M, Huntley B, Muller H, 1994. Eemian climate fluctuations observed in a European pollen record. *Nature*, 371(6500): 779–783. doi: 10.1038/371779a0

Folk R L, Ward C, 1957. Brazos River Bar: A study in the significance of grain size parameters. *Journal of Sedimentary Petrology*, 27(1): 3–26.

Fronval T, Jansen E, 1996. Rapid changes in ocean circulation and heat flux in the Nordic seas during the last interglacial period. *Nature*, 383(6603): 806–810. doi: 10.1038/383806a0

Frogley M R, Tzedakis P C, Heaton T H E, 1999. Climate variability in Northwest Greece during the Last Interglacial. *Science*, 285(5435): 1886–1889. doi: 10.1126/science.285.5435.1886

Gao Shangyu, Chen Weinan, Jin Heling *et al.*, 1993. Preliminary study of desert evolution in the monsoonal area of western China during the Holocene. *Science in China* (*Series B*), 23(2): 202–208. (in Chinese)

Grootes P M, Stuiver M, White J W C *et al.*, 1993. Comparison of oxygen isotope records from the GISP2 and GRIP Greenland ice cores. *Nature*, 366(6455): 552–554. doi: 10.1038/366552a0

GRIP Members, 1993. Climate instability during the last interglacial period recorded in the GRIP ice core. *Nature*, 371(6434): 779–783. doi: 10.1038/364203a0

Guan Donghong, Xi Xiaoxia, Hao Yongping *et al.*, 1996. Climate instability revealed in the Beiyuan $CaCO_3$ record during the

last interglacial age. *Journal of Glaciology and Geocryology*, 18(2): 119–124. (in Chinese)

Guan Q Y, Pan B T, Gao H S *et al.*, 2007. Instability characteristics of the East Asian Monsoon recorded by high-resolution loess sections from the last interglacial (MIS5). *Science in China* (*Series D*), 50(7): 1067–1075. doi: 10.1007/s11430-007-0040-x

Konert M, Vandenberghe J, 1997. Comparison of laser grain size analysis with pipette and sieve analysis: A solution for the underestimation of the clay fraction. *Sedimentology*, 44(3): 523–535. doi: 10.1046/j.1365-3091.1997.d01-38.x

Krumbein W C, Pettijohn F J, 1938. *Manual of Sedimentary Petrography*. New York: Appleton-Century.

Li B S, Zhang D D, Jin H L *et al.*, 2000. Paleo-monsoon activities of Mu Us Desert, China since 150 kyr B P: A study of the stratigraphic sequences of the Milanggouwan Section, Salawusu River area. *Palaeogeography*, *Palaeoclimatology*, *Palaeoecology*, 162(1–2): 1–16. doi: 10.1016/S0031-0182(00)00101-2

Linsley B K, 1996. Oxygen-isotope record of sea level and climate variations in the Sulu Sea over the past 150,000 years. *Nature*, 380(6571): 234–237. doi: 10.1038/380234a0

Liu D S, 1985. *Loess and Environments*. Beijing: Science Press.

Liu X M, Hesse P, Liu T S *et al.*, 1998. High resolution climate record from the Beijing area during the last glacial-interglacial cycle. *Geophysical Research Letters*, 25(3): 349–352. doi: 10.1029/97GL03713

Lu Yingxia, Li Baosheng, Wen Xiaohao *et al.*, 2010. Millennial-centennial scales climate changes of Holocene indicated by magnetic susceptibility of high-resolution section in Salawusu River Valley, China. *Chinese Geographical Science*, 20(3): 243–251. doi: 10.1007/s11769-010-0243-5

Martinson D G, Pisias N G, Hays J D *et al.*, 1987. Age dating and the orbital theory of the ice ages: Development of a high-resolution 0 to 300,000-year chronostratigraphy. *Quaternary Research*, 27(1): 1–29. doi: 10.1016/0033-5894(87)90046-9

Mayewski P A, Meeker L D, Twickler M S *et al.*, 1997. Major features and forcing of high latitude northern hemisphere atmospheric circulation using a 110,000-year long glaciochemical series. *Journal of Geophysical Research*, 102(26): 345–366. doi: 10.1029/96JC03365

NGRIP Members, 2004. High-resolution record of northern hemisphere climate extending into the last interglacial period. *Nature*, 431(7005): 147–151. doi: 10.1038/nature02805

Qiang Mingrui, Li Sen, Gao Shangyu, 2004. Evidence for abrupt climatic changes on northwestern margin of east Asian monsoon region during last deglaciation. *Chinese Geographical Science*, 14(2): 117–121. doi: 10.1007/s11769-004-0018-y

Ren J Z, Ding Z L, Liu T S *et al.*, 1996. Climatic changes on millennial time scale—Evidence from a high-resolution loess record. *Sciciene in China* (*Series D*), 39(5): 449–459.

Rioual P, Andrieu-Ponel V, Rietti-Shati M *et al.*, 2001. High-resolution record of climate stability in France during the last interglacial period. *Nature*, 413(6853): 293–296. doi: 10.1038/35095037

Rousseau D D, Hatte C, Guiot J *et al.*, 2006. Reconstruction of the Grande Pile Eemian using inverse modeling of biomes and $\delta^{13}C$. *Quaternary Science Reviews*, 25(21–22): 2806–2819. doi: 10.1016/j.quascirev.2006.06.011

Stuiver M, Braziunas T, 1993. Sun, ocean, climate and atmospheric $^{14}CO_2$: An evaluation of causal and spectral relationships. *Holocene*, 3(4): 289–305. doi: 10.1177/095968369300300401

Taylor K, Hammer C, Alley R *et al.*, 1993. Electrical conductivity measurements from the GISP2 and GRIP Greenland ice cores. *Nature*, 366(6455): 549–552. doi: 10.1038/366549a0

Thouveny N, de Beaulieu J L, Bonifay E *et al.*, 1994. Climate variations in Europe over the past 140 kyr deduced from rock magnetism. *Nature*, 371(6497): 503–506. doi: 10.1038/371503a0

Wang Y J, Cheng H, Edwards R L *et al.*, 2001. A high-resolution absolute-dated Late Pleistocene monsoon record from Hulu Cave, China. *Science*, 294(5550): 2345–2348. doi: 10.1126/science. 1064618

Wen X H, Li B S, Zheng Y M *et al.*, 2009. Climate variability in the Salawusu River valley of the Ordos Plateau (Inner Mongolia, China) during Marine Isotope Stage 3. *Journal of Quaternary Science*, 24(1): 61–74. doi: 10.1002/jqs.1180

Zagwijn W H, 1996. An analysis of Eemian climate in western and central Europe. *Quaternary Science Reviews*, 15(5–6): 451–469. doi: 10.1016/0277-3791(96)00011-X

Zhang Pingzhong, Wang Xianbin, Wang Sumin *et al*., 1998. Climate instability during the Last Interglacial in eastern part of Qinghai-Xizang plateau. *Chinese Science Bulletin*, 43(1): 17–21. (in Chinese)